Optimal reference polarization states for the calibration of general Stokes polarimeters in the presence of noise

Tingkui Mu *, Donghao Bao, Chunmin Zhang, Zeyu Chen, Jionghui Song

School of Science, Xi'an Jiaotong University, Xi'an, Shaanxi 710049, PR China
Key Laboratory for Nonequilibrium Synthesis and Modulation of Condensed Matter (Xi'an Jiaotong University), Ministry of Education, Xi'an, Shaanxi 710049, PR China

A B S T R A C T

During the calibration of the system matrix of a Stokes polarimeter using reference polarization states (RPSs) and pseudo-inversion estimation method, the measurement intensities are usually noised by the signal-independent additive Gaussian noise or signal-dependent Poisson shot noise, the precision of the estimated system matrix is degraded. In this paper, we present a paradigm for selecting RPSs to improve the precision of the estimated system matrix in the presence of both types of noise. The analytical solution of the precision of the system matrix estimated with the RPSs are derived. Experimental measurements from a general Stokes polarimeter show that accurate system matrix is estimated with the optimal RPSs, which are generated using two rotating quarter-wave plates. The advantage of using optimal RPSs is a reduction in measurement time with high calibration precision.

1. Introduction

Stokes polarimeters, also termed as polarization state analyzers (PSAs), are powerful tools for characterizing the states of polarization of target [1–3]. To get full Stokes parameters $[S_0, S_1, S_2, S_3]$, a PSA should have $N_B \geq 4$ different analysis states, and these states form a so-called system matrix B with a dimension of $N_B \times 4$ [1]. Before using the PSA for practical measurement, its practical system matrix B needs to be estimated using a polarization state generator (PSG) that generates $N_A \geq 4$ different reference polarization states (RPSs) [4,5]. These states form a RPS matrix A with a dimension of $N_A \times 4$. The system matrix B is estimated using pseudo-inversion estimation of the well-known RPS matrix A and the measured intensity matrix I with a dimension of $N_A \times N_B$. The RPS method for calibration has the potential of accounting for higher order effects of systematic errors such as multiple reflections between or within optical devices, incorrectly oriented crystals in retarders, imperfect polarizers, and residual birefringence [4,5]. However, there are no guide theory for the selection of RPSs. Most of RPSs are generated using a simple PSG setup of easy implementation [6–10].

It is noted that the intensities, measured by the PSA during calibration, usually are perturbed by several types of noise such as signal-independent detector noise, signal-dependent shot noise, or compound noise [11]. The estimation precision of the system matrix is then limited by noisy data. Up to now, most researches only focus on the optimization of the PSA's analysis states in the presence of noise [12–21]. For

example, the optimal estimation of samples' Muller matrix by selecting PSG and PSA in the presence of both Gaussian and Poisson noise are presented [21]. The closed-form solutions of estimation precision show that the optimal PSG and PSA architectures that minimize and equalize the estimation variances of the sample's Muller matrix are based on spherical designs of order 2 or 3. These spherical designs have ever been identified analytically [14–16] and numerically [17–19] during the optimization of the PSA [10–12]. A spherical design of order t is a set of N_A points on the surface of the unit sphere for which the normalized integral of any polynomial of degree t or less is equal to the average taken over the N_A points [14]. The platonic solids such as tetrahedron, octahedron, cube, icosahedron, dodecahedron all belong to spherical designs [16,17].

However, to our best knowledge, the choice of RPSs for minimizing and equalizing the estimation variance of the system matrix of a general PSA has not been explored, and the corresponding estimation performance remains to be quantified. In this paper, we will estimate the practical system matrix of a general PSA in linear optics with pseudo-inversion method. The closed-form expressions of the estimation precision in the presence of both Gaussian and Poisson noise are derived. It is demonstrated that, for calibrating arbitrary system matrix (regardless of optimal ones [12–19], or not [8,22–27]), the optimal RPSs that can minimize and equalize noise variance are based on spherical designs of order 2 or 3. The important feature of the optimal RPSs is

that the sum of the matrix elements of any columns is equal to zero except for the first column. We verify the analytical solutions with Monte Carlo simulations and experiments at first time. The architectures for generating the optimal RPSs are presented. Experimental results show that the system matrix estimated with the proposed RPSs has immunity to kinds of noise such as, but not limit to, Gaussian and Poisson noise.

2. Theory

2.1. Calibration model

The calibration system usually comprises an unpolarized light source with intensity I_0, a PSG and a PSA. The RPSs and analysis states generated by the PSG and PSA, respectively, are stacked row-wise to form the RPS matrix A and the system matrix B. The matrix A (B) thus has the dimensions $N_A \times 4$ ($N_B \times 4$). The intensities acquired by the PSA are

$$I = I_0 BA^T, \tag{1}$$

where I is a $N_B \times N_A$-dimensional intensity matrix representing $N_B N_A$ measurements, and the superscript T indicates transpose. In the following, we will estimate the system matrix $I_0 B$, and define a vector operator by stacking the matrix elements row-wise to form a vector. Then Eq. (1) is rewritten as

$$\mathbf{V}_I = [E \otimes A]\mathbf{V}_B, \tag{2}$$

where $\otimes$ represents the Kronecker product [28], E is a $N_B \times N_B$-dimensional identity matrix, $\mathbf{V}_B = ([V_B]_1, \dots, [V_B]_{4N_B})$ is a $4N_B$-dimensional analysis state vector, and $\mathbf{V}_I = ([V_I]_1, \dots, [V_I]_{N_A N_B})$ is a $N_A N_B$-dimensional intensity vector by reading the corresponding matrix elements in the lexicographic order.

In this paper, we consider that the measurement vector $\mathbf{V}_I$ is disturbed by two types of common noise sources: additive Gaussian noise or Poisson shot noise, respectively. The analysis state vector $\mathbf{V}_B$ is estimated from the noisy measurements using pseudo-inverse (PI) estimator $\hat{\mathbf{V}}_B$ [21],

$$\hat{\mathbf{V}}_B = P\mathbf{V}_I \text{ with } P = \left([E \otimes A]^T [E \otimes A]\right)^{-1} [E \otimes A]^T, \tag{3}$$

where P is the pseudoinverse of the $4N_B \times N_A N_B$-dimensional matrix $[E \otimes A]$. Based the properties of the Kronecker product [26], the PI matrix is rewritten as

$$P = [G_E \otimes G_A][E \otimes A]^T, \tag{4}$$

where $G_U = (U^T U)^{-1}$ with $U = E$ or A.

The pseudo-inverse estimator $\hat{\mathbf{V}}_B$ is the best possible estimator and unbiased in the presence of Gaussian or Poisson noise. Its precision is indicated by its covariance matrix [21].

$$\Gamma_{\mathbf{V}_B} = P\Gamma_{\mathbf{V}_I}P^T. \tag{5}$$

A standard scalar performance criterion for polarization calibration is the sum of the variances of all the elements of the system matrix, which is the trace of $\Gamma_{\mathbf{V}_B}$ [21]:

$$\Omega = \text{Tr}[P\Gamma_{\mathbf{V}_I}P^T]. \tag{6}$$

2.2. Gaussian noise

We first assume that the measurements are mainly perturbed by zero-mean additive white Gaussian noise with variance σ^2. The covariance matrix in Eq. (5) of the estimator should be [21]

$$\Gamma_{\mathbf{V}_B} = \sigma^2[G_E \otimes G_A], \tag{7}$$

and the criterion in Eq. (6) is deduced as

$$\Omega^{\text{gau}} = \sigma^2 \text{Tr}[G_E]\text{Tr}[G_A], \tag{8}$$

where $\text{Tr}[G_E] = \text{Tr}[E] = N_B$ is a constant. Obviously, the total variance does not depend on the observed system matrix itself. Our aim is to find optimal RPS matrix A for minimizing the performance criterion Ω^{gau}, thus minimizing $\text{Tr}[G_A]$. It has been shown that $\text{Tr}[G_A]$ is minimized if the last three columns of the RPS matrix A form a sphere 2 design on the Poincaré sphere of unit radius [14–16], that is $A^T A = \frac{N_A}{12}\text{diag}(3,1,1,1)$ and $G_A = \frac{4}{N_A}\text{diag}(1,3,3,3)$. Then the matrix $G_E \otimes G_A$ in Eq. (7) is a $4N_B \times 4N_B$-dimensional diagonal matrix, and its coefficients $[G_E \otimes G_A]_{ii}$ are derived as

$$\begin{cases} 4/N_A & \text{if } i = 4m+1, \text{ and } m = 0, 1, \dots, N_B - 1 \\ 12/N_A & \text{others.} \end{cases} \tag{9}$$

The corresponding minimal value of the performance criterion is calculated as

$$\Omega^{\text{gau}}_{\text{opt}} = \frac{40N_B}{N_A}\sigma^2. \tag{10}$$

As seen, the total noise variance decreases with the increase of the number of the RPSs when the numbers of the analysis states are fixed. The covariance matrix $\Gamma_{\mathbf{V}_B}$ in Eq. (7) is diagonal and its diagonal elements denote the estimation variances of the elements of the system matrix B as

$$\text{VAR}[B]^{\text{gau}}_{\text{opt}} = \frac{4}{N_A}\sigma^2 \begin{bmatrix} 1 & 3 & 3 & 3 \\ 1 & 3 & 3 & 3 \\ \vdots & \vdots & \vdots & \vdots \\ 1 & 3 & 3 & 3 \end{bmatrix}_{N_B \times 4}. \tag{11}$$

It is interesting to note that the variance of each element is also independent of the observed system matrix B, and its last three columns achieve noise equalization.

2.3. Poisson noise

Second, we assume that the measurements are mainly degraded by Poisson shot noise. The diagonal element of the covariance matrix $\Gamma_{\mathbf{V}_B}$ in Eq. (5) is derived as [21]

$$\forall i \in [1, 4N_B], [\Gamma_{\mathbf{V}_B}]_{ii} = \sum_{j=1}^{4N_B} Q_{ij}[\mathbf{V}_B]_j, \tag{12}$$

where Q is a $4N_B \times 4N_B$-dimensional matrix expressed as

$$\forall (i,j) \in [1, 4N_B], \ Q_{ij} = \sum_{n=1}^{N_A N_B} (P_{in})^2 [E \otimes A]_{nj}. \tag{13}$$

It is easily found that the variances depend on the observed system matrix B in the presence of Poisson noise, which are different from the case in Eq. (7) in the presence of Gaussian noise. The performance criterion in Eq. (6) is then given as [21]

$$\Omega^{\text{poi}} = \sum_{i=1}^{4N_B} [\Gamma_{\mathbf{V}_B}]_{ii} = \mathbf{V}_{(E,A)}^T \mathbf{V}_B, \tag{14}$$

where $\mathbf{V}_{(E,A)}$ is a $4N_B$-dimensional vector defined as

$$\forall j \in [1, 4N_B], [\mathbf{V}_{(E,A)}]_j = \sum_{i=1}^{4N_B} Q_{ij}. \tag{15}$$

If the RPSs form a sphere 3 design on the Poincaré sphere [21], one derives

$$Q_{ij} = \begin{cases} 1/N_A & \text{if } i = m \cdot 4 + 1, \text{ and } m = 0, 1, \dots, N_B - 1 \\ 3/N_A & \text{others.} \end{cases} \tag{16}$$

Then the optimal value of the performance criterion is derived as

$$\Omega^{\text{poi}}_{\text{opt}} = \frac{40N_B}{N_A}\frac{I_0}{4}. \tag{17}$$

It is found that $\Omega_{\text{opt}}^{\text{poi}}$ in Eq. (17) has the same expression as $\Omega_{\text{opt}}^{\text{gau}}$ in Eq. (10), with variance σ^2 replaced by $I_0/4$. Similarly, the total noise variance decreases with the increase of the numbers of the RPSs if the numbers of the analysis states are fixed. The variances of the elements of the system matrix B, ordered in the matrix VAR[B], are

$$\text{VAR}[B]_{\text{opt}}^{\text{poi}} = \frac{4}{N_A} \frac{I_0}{4} \begin{bmatrix} 1 & 3 & 3 & 3 \\ 1 & 3 & 3 & 3 \\ \vdots & \vdots & \vdots & \vdots \\ 1 & 3 & 3 & 3 \end{bmatrix}_{N_B \times 4}. \tag{18}$$

It is interesting to note that the VAR[B]$_{\text{opt}}^{\text{poi}}$ in Eq. (18) has the same expression as the VAR[B]$_{\text{opt}}^{\text{gau}}$ in Eq. (11), with variance σ^2 replaced by $I_0/4$.

3. Monte Carlo simulations

To verify the proposed method, the theoretical results obtained above is particularized for a general Stokes polarimeter with the system matrix

$$B = \frac{1}{2} \begin{bmatrix} 1 & 1 & 0 & 0 \\ 1 & -1 & 0 & 0 \\ 1 & 0 & 1 & 0 \\ 1 & 0 & 0 & 1 \end{bmatrix}. \tag{19}$$

This system matrix is formed using linear polarizers at 0°, 90°, 45° and a right circular polarizer [1]. It is widely employed in practice [23–26]. However, it is not an optimal Stokes polarimeter; since the L_2 norm condition number of the system matrix is about 3.2255, larger than ideal value of $\sqrt{3}$ [12–19]. In the simulation, we assume there is no any systematic error in the practical Stokes polarimeter, and the measured intensities are only influenced by Gaussian or Poisson noise during calibration. This is not true in real case, because the system matrix will deviate from ideal one due to the systematic errors such as alignment error and retardance error. This point is discussed further in Section 4 below.

To compare the influence of noise on the estimated system matrix, six different RPS matrices are employed to estimate the system matrix from simulated noisy intensities, respectively. Assuming the first RPS matrix A_1 is the same to the system matrix, that is $A_1 = B$. The second one A_2 forms a regular tetrahedron (sphere 2 design) on the Poincaré sphere [6], that is $A_2 = 0.5[1, a, b, c; 1, -a, -b, -c; 1, a, -c, b; 1, a, c, -b]$, where $a = 1/\sqrt{3}$, $b = 0.1877$, $c = 0.3626$. The third one A_3 forms a regular tetrahedron (sphere 2 design) with a specific orientation [7,11,12], that is $A_3 = 0.5[1, a, a, a; 1, a, -a, -a; 1, -a, -a, a; 1, -a, a, -a]$. The fourth one A_4 forms a regular octahedron (sphere 3 design) based on linear polarizers at 0°, 90°, 45°, 135°, and right- and left-circular polarizers [8,9], that is $A_4 = 0.5[1, 1, 0, 0; 1, -1, 0, 0; 1, 0, 1, 0; 1, 0, -1, 0; 1, 0, 0, 1; 1, 0, 0, -1]$. The fifth matrix A_5 forms a regular cube and the sixth matrix A_6 forms an icosahedron, which all belong to sphere 3 design.

For these six RPSs matrices, we compute the performance criterion Ω and the variance matrix VAR[B] by using the analytical forms in the presence of Gaussian noise with zero mean and variance $\sigma^2 = 0.1$ (see Eqs. (7) and (8)), and Poisson noise, (see Eqs. (12) and (14)). The theoretical results are shown in Table 1. We have checked the validity of theoretical prediction with Monte Carlo simulations. It is found that when a sufficient number of realizations for each intensity is used, all simulation results have a very good agreement with theoretical values. With the 10^5 random realizations in the Monte Carlo simulation, the relative differences between the theoretical and simulated results are less than 1.2% for the variance of each element and 0.8% for the sum of the variances of all the elements.

We observe that the performance criterion Ω is minimal for the RPS matrices A_2 and A_3 because they form the regular tetrahedrons on the Poincaré sphere regardless of their orientations. In contrast, for the general RPS matrix A_1, the total variance is relatively larger for both Gaussian and Poisson noise. Let us now look at the variances VAR[B]

of the different elements of the system matrix. The variances for the matrix A_1 are diverse for both types of noise. For the general tetrahedron matrix A_2, the variances along the last three columns are similar only for Gaussian noise, but diverse for Poisson noise. In contrast, for the RPS matrix A_3, the variances along the last three columns are similar for both types of noise because A_3 forms the regular tetrahedron with a special orientation. Since the RPS matrices A_4, A_5 and A_6 belong to sphere 3 design, both the performance criterion Ω and the variances VAR[B] achieve optimization in the presence of both types of noise. Obviously, for the same number of RPSs, the optimal sets of RPSs can realize the minimization and equalization of the noise variance in the estimated system matrix compared to the nonoptimal sets of RPSs.

4. Experimental verification

4.1. PSG

Previously, we have optimized a full-Stokes polarimeter that consists of two rotatable quarter waveplates (QWPs) followed by a fixed horizontally linear polarizer [18,19]. The optimal sets of fast axis directions of the two QWPs are determined at different numbers N_B of analysis states such as $N_B = 4, 6, 8, 12$ and 20. These analysis states correspond to the Platonic solids such as tetrahedron, octahedron, cube, icosahedron, and dodecahedron respectively [19]. It is noted that the PSG can be built easily by reversing the configuration of the optimized full-Stokes polarimeter. As shown in Fig. 1, the PSG consists of a fixed horizontally linear polarizer P1 followed by the QWP1 and QWP2 in tandem. The optimal sets of fast axis azimuths (θ_1, θ_2) of the two QWPs and the corresponding RPS matrices of the Platonic solids such as tetrahedron with two special directions, octahedron and cube are derived in Table 2. In this paper, for simplification, we just use the first tetrahedron I and the octahedron in Table 2 to calibrate the system matrix of a general PSA, respectively, for comparison.

4.2. PSA

In Fig. 1, a general PSA consists of a rotatable QWP3 followed by a fixed horizontally linear polarizer P2 will act as a full Stokes polarimeter. Diverse analysis states can be generated by rotating the QWP3 to different sets of azimuth angles. As an example, we will rotate the QWP3 to a set of azimuth angles [−45°, 0°, 30°, 60°], the corresponding system matrix is [29]

$$B_{\text{ideal}} = \frac{1}{2} \begin{bmatrix} 1.0000 & 0.0000 & 0.0000 & 1.0000 \\ 1.0000 & 1.0000 & 0.0000 & 0.0000 \\ 1.0000 & 0.2500 & 0.4330 & -0.8660 \\ 1.0000 & 0.2500 & -0.4330 & -0.8660 \end{bmatrix}. \tag{20}$$

This PSA is a non-optimal configuration, since the L_2 condition number of the system matrix B is about 3.6268 that is larger than $\sqrt{3}$. The matrix in Eq. (20) is theoretical and ideal one. In fact, the system matrix will deviate from the theoretical one due to imperfect optical elements or other factors [30–32]. Therefore, the real system matrix should be calibrated first before using it in practical application.

4.3. Experimental setups

Figure 2 shows our experimental setup. The PSG consists of a horizontally linear polarizer (CVI Melles Griot, FPG-50.8-5.3) and two rotatable free-standing polymeric achromatic QWP1 and QWP2 (BVO Inc., AQWP-25.4) in tandem. The QWPs can be automatically rotated via two continuous 360° motorized rotation stages (Thorlabs, KPRM1E/M) respectively. The PSA comprises a free-standing polymeric achromatic QWP3 (BVO Inc., AQWP-25.4) followed by a horizontally linear polarizer. The QWP3 can be manually rotated via a continuous 360° manually operated rotation stage. Light beam emitted from a linearly polarized He–Ne laser first pass through a rotatable Glan–Taylor polarizer P0 for

Table 1

Variance of each element of the system matrix and efficiency criterion values obtained by using different sets of RPS matrices. A_1 is the same to the system matrix B. A_2 forms a general tetrahedron. A_3 forms a tetrahedron with the specific orientation. A_4 forms an octahedron. A_5 forms a cube. A_6 forms an icosahedron.

	A_1	A_2	A_3
$\mathrm{VAR}[B]_{\mathrm{opt}}^{\mathrm{gau}} = \sigma^2 \times$	$\begin{bmatrix} 2.01 & 1.99 & 6.00 & 6.01 \\ 2.00 & 2.00 & 6.02 & 5.99 \\ 2.00 & 2.01 & 6.01 & 6.00 \\ 2.00 & 2.00 & 6.00 & 5.99 \end{bmatrix}$	$\begin{bmatrix} 1 & 3 & 3 & 3 \\ 1 & 3 & 3 & 3 \\ 1 & 3 & 3 & 3 \\ 1 & 3 & 3 & 3 \end{bmatrix}$	$\begin{bmatrix} 1 & 3 & 3 & 3 \\ 1 & 3 & 3 & 3 \\ 1 & 3 & 3 & 3 \\ 1 & 3 & 3 & 3 \end{bmatrix}$
$\Omega_{\mathrm{opt}}^{\mathrm{gau}} = \sigma^2 \times$	64.05	40.10	40.14
$\mathrm{VAR}[B]_{\mathrm{opt}}^{\mathrm{poi}} = \frac{I_0}{4} \times$	$\begin{bmatrix} 2.00 & 2.00 & 6.00 & 6.00 \\ 1.99 & 1.99 & 5.97 & 5.99 \\ 2.00 & 2.00 & 9.99 & 6.03 \\ 1.99 & 2.00 & 6.00 & 9.94 \end{bmatrix}$	$\begin{bmatrix} 1.02 & 2.86 & 3.82 & 1.97 \\ 1.04 & 3.15 & 1.98 & 4.15 \\ 0.94 & 3.38 & 2.77 & 3.25 \\ 0.99 & 3.03 & 3.28 & 2.97 \end{bmatrix}$	$\begin{bmatrix} 1 & 3 & 3 & 3 \\ 1 & 3 & 3 & 3 \\ 1 & 3 & 3 & 3 \\ 1 & 3 & 3 & 3 \end{bmatrix}$
$\Omega_{\mathrm{opt}}^{\mathrm{poi}} = \frac{I_0}{4} \times$	71.90	40.60	40.21
	A_4	A_5	A_6
$\mathrm{VAR}[B]_{\mathrm{opt}}^{\mathrm{gau}} = \sigma^2 \times$	$\frac{2}{3}\begin{bmatrix} 1 & 3 & 3 & 3 \\ 1 & 3 & 3 & 3 \\ 1 & 3 & 3 & 3 \\ 1 & 3 & 3 & 3 \end{bmatrix}$	$\frac{1}{2}\begin{bmatrix} 1 & 3 & 3 & 3 \\ 1 & 3 & 3 & 3 \\ 1 & 3 & 3 & 3 \\ 1 & 3 & 3 & 3 \end{bmatrix}$	$\frac{1}{3}\begin{bmatrix} 1 & 3 & 3 & 3 \\ 1 & 3 & 3 & 3 \\ 1 & 3 & 3 & 3 \\ 1 & 3 & 3 & 3 \end{bmatrix}$
$\Omega_{\mathrm{opt}}^{\mathrm{gau}} = \sigma^2 \times$	26.62	20.05	13.32
$\mathrm{VAR}[B]_{\mathrm{opt}}^{\mathrm{poi}} = \frac{I_0}{4} \times$	$\frac{2}{3}\begin{bmatrix} 1 & 3 & 3 & 3 \\ 1 & 3 & 3 & 3 \\ 1 & 3 & 3 & 3 \\ 1 & 3 & 3 & 3 \end{bmatrix}$	$\frac{1}{2}\begin{bmatrix} 1 & 3 & 3 & 3 \\ 1 & 3 & 3 & 3 \\ 1 & 3 & 3 & 3 \\ 1 & 3 & 3 & 3 \end{bmatrix}$	$\frac{1}{3}\begin{bmatrix} 1 & 3 & 3 & 3 \\ 1 & 3 & 3 & 3 \\ 1 & 3 & 3 & 3 \\ 1 & 3 & 3 & 3 \end{bmatrix}$
$\Omega_{\mathrm{opt}}^{\mathrm{poi}} = \frac{I_0}{4} \times$	26.68	20.03	13.35

Table 2

The azimuths of the QWP1 and QWP2 for the realization of the Platonic solids, and the corresponding ideal RPS matrices.

N_A	Platonic solids	Azimuths $(\theta_1, \theta_2)/°$	RPS matrix A_{ideal}
4	Tetrahedron-I	(−64.66, +58.18) (+64.66, −58.18) (+70.86, +47.18) (−70.86, −47.18)	$\frac{1}{2}\begin{bmatrix} 1 & +1/\sqrt{3} & +1/\sqrt{3} & +1/\sqrt{3} \\ 1 & +1/\sqrt{3} & -1/\sqrt{3} & -1/\sqrt{3} \\ 1 & -1/\sqrt{3} & -1/\sqrt{3} & +1/\sqrt{3} \\ 1 & -1/\sqrt{3} & +1/\sqrt{3} & -1/\sqrt{3} \end{bmatrix}$
4	Tetrahedron-II	(−19.14, −42.82) (+19.14, +42.82) (−87.84, −70.15) (+87.84, +70.15)	$\frac{1}{2}\begin{bmatrix} 1 & -1/\sqrt{3} & -1/\sqrt{3} & -1/\sqrt{3} \\ 1 & -1/\sqrt{3} & +1/\sqrt{3} & +1/\sqrt{3} \\ 1 & +1/\sqrt{3} & +1/\sqrt{3} & -1/\sqrt{3} \\ 1 & +1/\sqrt{3} & -1/\sqrt{3} & +1/\sqrt{3} \end{bmatrix}$
6	Octahedron	(+45, −20) (−45, −20) (−45, +25) (+45, +25) (0, +45); (0, −45)	$\frac{1}{2}\begin{bmatrix} 1 & +0.6428 & +0.7660 & 0 \\ 1 & -0.6428 & -0.7660 & 0 \\ 1 & +0.7660 & -0.6428 & 0 \\ 1 & -0.7660 & +0.6428 & 0 \\ 1 & 0 & 0 & +1 \\ 1 & 0 & 0 & -1 \end{bmatrix}$
8	Cube	(+45, +22) (−45, −22) (+45, −22) (−45, +22) (+12.6, −45) (+12.7, +45) (−12.6, +45) (−12.7, −45)	$\frac{1}{2}\begin{bmatrix} 1 & -0.6947 & +0.7193 & 0 \\ 1 & -0.6947 & -0.7193 & 0 \\ 1 & +0.6947 & +0.7193 & 0 \\ 1 & +0.6947 & -0.7193 & 0 \\ 1 & +0.4258 & +0.3853 & -0.8187 \\ 1 & -0.4289 & +0.3875 & +0.8160 \\ 1 & +0.4258 & -0.3853 & +0.8187 \\ 1 & -0.4289 & -0.3875 & -0.8160 \end{bmatrix}$
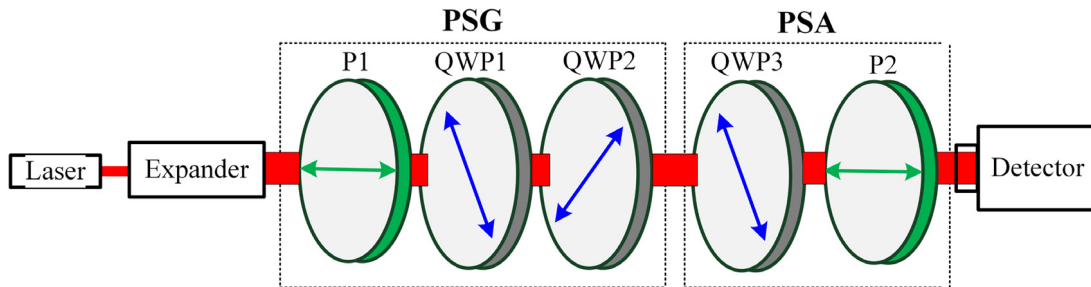
Fig. 1. The optical schema for the verification of the calibration strategy.
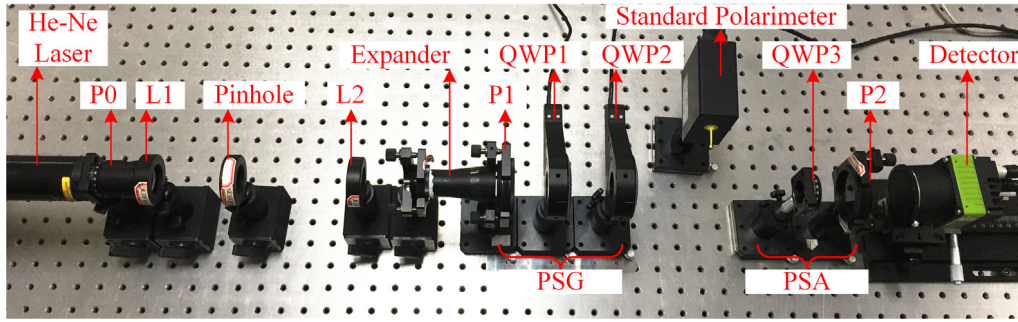
Fig. 2. Experimental setup for the calibration verification.

tuning the beam power. By rotating the P0 to a special position, all of measurements will not have any saturated pixels. Then the beam is focused by the first lens L1. A pinhole located at focal plane of the lens L1 is used to filter out unwanted nonuniformly beam. The divergent beam from the pinhole is collimated by the second lens L2 and expanded by a 5× beam expander. The widen beam passes through the PSG and PSA, and finally arrives at a CMOS camera (JAI, SP-20000M-MLC) directly without any auxiliary lens. A relatively uniform light spot that covers about 120×120 pixel are formed on the CMOS.

Since the retardations of the achromatic QWPs are not the ideal value of 90° at the wavelength of 632.8 nm, the real RPS matrices of the PSG will deviate from the ideal ones shown in Table 2. To get the well-known RPS matrices, a standard polarimeter (Thorlabs, PAX1000VIS) is employed to measure the Stokes parameters generated by the PSG. The standard polarimeter is based on a continuously rotating quarter-wave plate technique, and the Fourier analysis is used to recover the Stokes parameters. With the rotation of the QWP1 and QWP2 following the azimuthal angles in Table 2, more than 10^3 measurements are realized by the polarimeter (Thorlabs, PAX1000VIS) at each RPS for averaging. Finally, the practical RPS matrix of the PSG for the tetrahedron I is measured as

$$A_{\mathrm{T,real}} = \frac{1}{2} \begin{bmatrix} 1.0000 & 0.6210 & 0.5913 & 0.5138 \\ 1.0000 & 0.5499 & -0.6123 & -0.5679 \\ 1.0000 & -0.5637 & -0.5769 & 0.5910 \\ 1.0000 & -0.5652 & 0.6056 & -0.5600 \end{bmatrix}. \tag{21}$$

The practical RPS matrix for the octahedron is

$$A_{\mathrm{O,real}} = \frac{1}{2} \begin{bmatrix} 1.0000 & 0.6229 & 0.7805 & 0.0520 \\ 1.0000 & -0.7240 & -0.6898 & 0.0054 \\ 1.0000 & 0.7178 & -0.6962 & 0.0080 \\ 1.0000 & -0.7887 & 0.6143 & -0.0212 \\ 1.0000 & -0.0296 & -0.0135 & 0.9995 \\ 1.0000 & 0.0124 & 0.0574 & -0.9983 \end{bmatrix}. \tag{22}$$

As seen, there are slight differences between the measured and ideal RPS matrices mainly due to the imperfect retarder components and alignment errors [30]. The practical condition numbers of the PSG for the tetrahedron-I in Eq. (21) and the octahedron in Eq. (22) are, respectively, 1.7933 and 1.7716. Both are approximate to $\sqrt{3}$. Therefore, the practical RPS matrix of the PSG can be regarded as the optimal one and used to calibrate the PSA.

Similarly, the system matrix of the PSA also will deviate from ideal one shown in Eq. (20). The practical system matrix also can be determined by the standard polarimeter (Thorlabs, PAX1000VIS) for comparison. Since the polarizer P1 and P2 are aligned well with the assistant of the standard polarimeter, we first let the laser beam pass through the horizontally polarizer P1 and then just pass through the QWP3. The Stokes parameters are measured at four azimuthal angles

$[-45°, 0°, 30°, 60°]$ as

$$B_{\mathrm{real}} = \frac{1}{2} \begin{bmatrix} 1.0000 & -0.0547 & 0.0276 & 0.9976 \\ 1.0000 & 0.9996 & 0.0021 & 0.0264 \\ 1.0000 & 0.2559 & 0.4638 & -0.8480 \\ 1.0000 & 0.2427 & -0.4196 & -0.8744 \end{bmatrix}. \tag{23}$$

The practical condition number of the PSA is about 3.5401 which is approximate to the ideal value of 3.6268. The measured system matrix in Eq. (23) will be compared to the system matrix, as follows, estimated with the RPS matrices in Eq. (21) or (22).

4.4. Results

Generally, if the source intensity is low enough, the dominant noise can be considered Gaussian distribution. In contrast, when the intensity of the source is strong enough, the dominant noise will be Poisson distribution [11]. Therefore, we will implement experiments at two different illumination levels. The exposure time of the CMOS is set to 100 μs. More than 10^5 measurements are realized for each RPS and each analysis state.

4.4.1. Strong photon flux

First, we let the maximum digital number (DN) value of the light that pass through the polarizer P1 of the PSG is about 4000 via rotating the Glan–Taylor polarizer P0. This DN value is large enough since the analog-to-digital converter of the CMOS is 12 bits. According to the Malus law, the scaling DN value of the unpolarized intensity I_0 that incident on the polarizer P1 in the PSG should be about 8000 if the polarizer P1 is perfect. Figure 3 shows sixteen probability distribution functions (PDFs) of the measured intensities when the RPSs matrix in Eq. (21) is used for calibration. It is noted that the intensities approximately obey normal distribution. Substituting these intensities and Eq. (21) into Eq. (3), the PDF of each element of the estimated system matrix are calculated in Fig. 4. Obviously, the variances in the last three columns achieve equalization, and they are nearly three times of the first column. The mean value of the system matrix is

$$B_{\mathrm{real}}^{\mathrm{T}} = I_1 \times \frac{1}{2} \begin{bmatrix} 0.9961 & -0.0532 & 0.0281 & 0.9952 \\ 1.0000 & 0.9966 & 0.0024 & 0.0255 \\ 0.9971 & 0.2543 & 0.4643 & -0.8478 \\ 0.9963 & 0.2452 & -0.4187 & -0.8786 \end{bmatrix}, \tag{24a}$$

where $I_1 = 8000.1$. As seen, the estimated system matrix is approximate to the one in Eq. (23) measured by the standard polarimeter. That means our calibration process is valid. Correspondingly, the variance of each element of the estimated system matrix is

$$\mathrm{VAR}[B_{\mathrm{real}}]_{\mathrm{opt}}^{\mathrm{T}} = I_2 \times \begin{bmatrix} 0.9816 & 2.9978 & 2.7743 & 3.2064 \\ 1.0000 & 3.0593 & 2.8816 & 3.1527 \\ 0.9837 & 3.0387 & 2.8987 & 3.0824 \\ 0.9919 & 2.9416 & 2.8607 & 3.2626 \end{bmatrix}, \tag{24b}$$
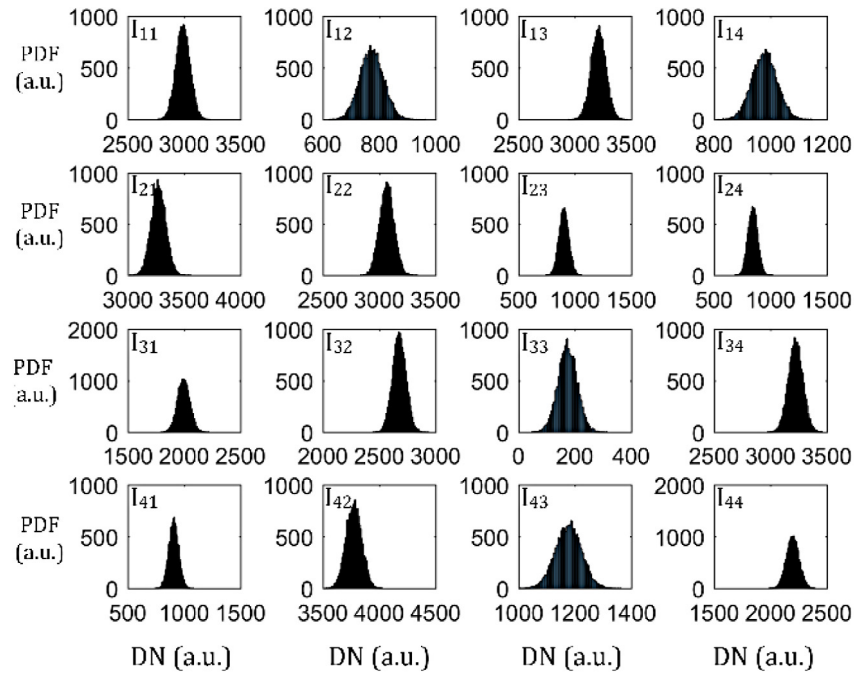
Fig. 3. The probability distributions functions (PDFs) of the measured intensities when using the RPSs of the tetrahedron with a relatively high illumination level.
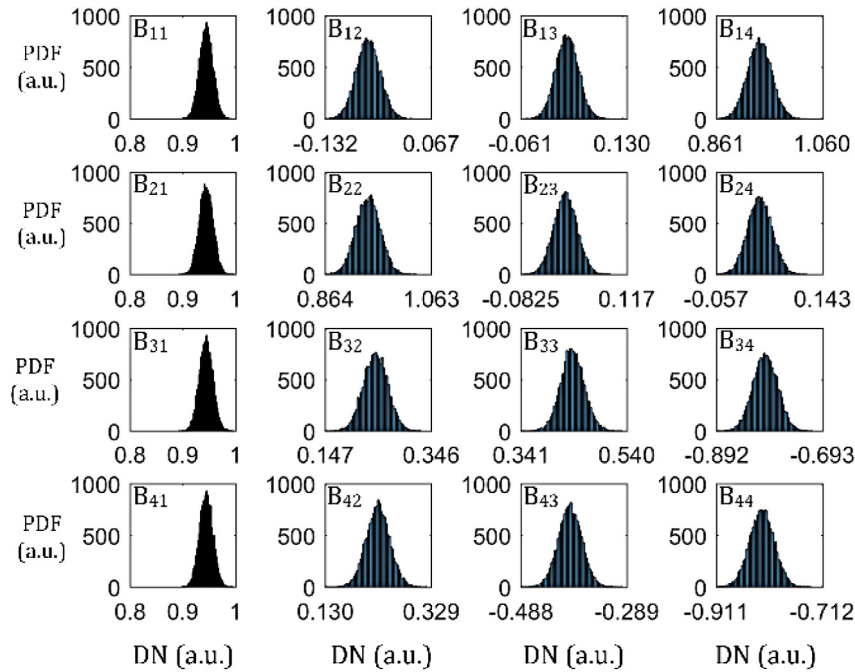

Fig. 4. The probability distributions functions (PDFs) of the elements of the estimated system matrix with normalized intensity.

where $I_2 = 2989.2$. The sum of the variances of all the elements of the estimated system matrix is

$$\Omega_{opt}^{T} = I_2 \times 40.11. \tag{24c}$$

The experimental results are consistent with the theoretical predictions. However, the coefficient I_2 in Eq. (24b) is different from the one that calculated from Eqs. (17) or (18). That means the total noise is not the pure Poisson noise as assumed, it is the combination of different types of noise. However, Poisson noise maybe dominant, since the coefficient in Eq. (18) is $I_0/4 = 2000$, which has the same order of magnitude to I_2.

Furthermore, we use the RPSs in Eq. (22) to calibrate the system matrix. The estimated results are:

$$B_{real}^{O} = I_3 \times \frac{1}{2}\begin{bmatrix} 0.9999 & -0.0541 & 0.0283 & 0.9960 \\ 0.9999 & 0.9987 & 0.0023 & 0.0253 \\ 1.0000 & 0.2572 & 0.4623 & -0.8495 \\ 0.9998 & 0.2407 & -0.4174 & -0.8726 \end{bmatrix}, \tag{25a}$$

$$\text{VAR}[B_{real}]_{opt}^{O} = I_4 \times \begin{bmatrix} 0.9932 & 2.9216 & 3.0857 & 2.9769 \\ 0.9875 & 2.8028 & 3.1504 & 2.9275 \\ 1.0000 & 2.8447 & 3.0241 & 3.0457 \\ 0.9826 & 2.8697 & 3.0045 & 2.9893 \end{bmatrix}, \tag{25b}$$
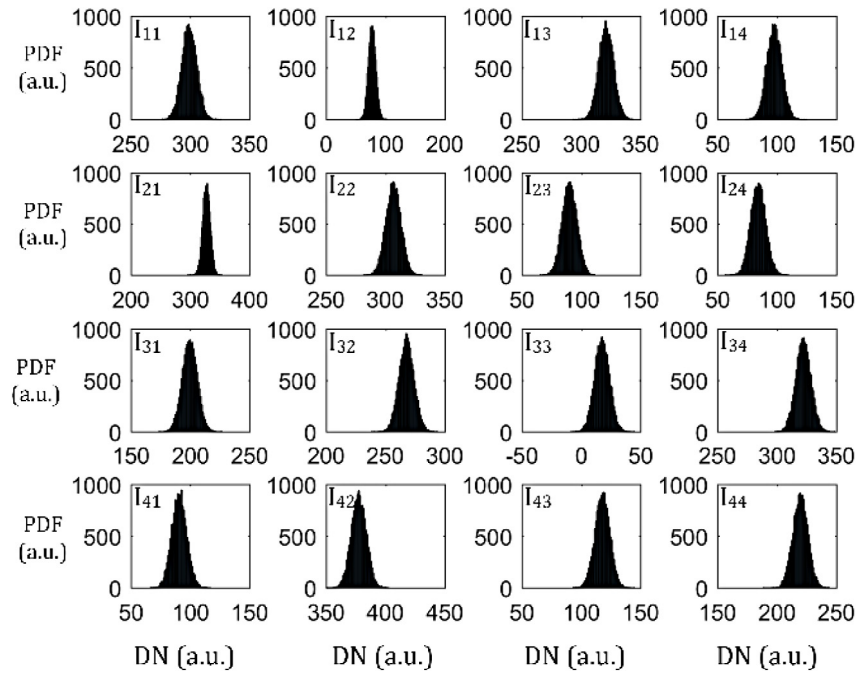
Fig. 5. The probability distributions function (PDF) of the measured intensities when using the RPSs of the tetrahedron with a low illumination level.

$$\Omega_{\text{opt}}^{\text{O}} = I_4 \times 39.61, \tag{25c}$$

where $I_3 = 8001.8$ and $I_4 = 2089.8$. Obviously, the estimated system matrix in Eq. (25a) is also approximate to that in Eq. (23) and the noise variances are optimized. Since I_4/I_2 is approximate to 2/3 which is consistent with the coefficient calculated from Eqs. (17) or (18), we can say that the total noise is dominant by the Poisson noise. This result confirms the above judgment. The main reason is that the photon flux of the system is large enough.

4.4.2. Low photon flux

Second, we let the maximum digital number (DN) value of the light that pass through the polarizer P1 of the PSG to be about 800. Correspondingly, intensity I_0 should be about 1600. Figure 5 shows sixteen probability distributions of the measured intensities when we use the RPSs matrix in Eq. (21). The intensities also approximately obey the normal distribution. The PDFs of each element of the estimated system matrix with normalized intensity are described in Fig. 6. The estimated results are:

$$B_{\text{real}}^{\text{T}} = I_5 \times \frac{1}{2} \begin{bmatrix} 1.0000 & -0.0537 & 0.0283 & 0.9980 \\ 0.9983 & 0.9981 & 0.0018 & 0.0271 \\ 1.0000 & 0.2564 & 0.4640 & -0.8477 \\ 0.9999 & 0.2422 & -0.4198 & -0.8735 \end{bmatrix}, \tag{26a}$$

$$\text{VAR}[B_{\text{real}}]_{\text{opt}}^{\text{T}} = I_6 \times \begin{bmatrix} 0.9952 & 3.0004 & 2.8060 & 3.2098 \\ 0.9868 & 3.0094 & 2.8257 & 3.1271 \\ 0.9739 & 2.9922 & 2.7831 & 3.2001 \\ 1.0000 & 3.0117 & 2.7729 & 3.1971 \end{bmatrix}, \tag{26b}$$

$$\Omega_{\text{opt}}^{\text{T}} = I_6 \times 39.89, \tag{26c}$$

where $I_5 = 800.2$ and $I_6 = 40.9$. As seen, the estimated system matrix in Eq. (26a) is also approximate to that in Eq. (23). The variances in the last three columns in Eq. (26b) achieve noise equalization and minimization, and they are nearly three times of that of the first column. Since coefficient I_6 in Eq. (26b) is far less than the illumination intensity I_0, the dominant noise maybe Gaussian distribution.

The RPSs in Eq. (22) was also used to estimate the system matrix, and the results are:

$$B_{\text{real}}^{\text{O}} = I_7 \times \frac{1}{2} \begin{bmatrix} 0.9996 & -0.0533 & 0.0278 & 0.9962 \\ 0.9986 & 0.9991 & 0.0025 & 0.0258 \\ 0.9997 & 0.2561 & 0.4627 & -0.8465 \\ 1.0000 & 0.2418 & -0.4187 & -0.8752 \end{bmatrix}, \tag{27a}$$

$$\text{VAR}[B_{\text{real}}]_{\text{opt}}^{\text{O}} = I_8 \times \begin{bmatrix} 1.0000 & 2.9113 & 3.0905 & 2.9355 \\ 0.9888 & 2.8211 & 3.0012 & 2.9454 \\ 0.9946 & 2.8643 & 3.9759 & 2.9570 \\ 0.9945 & 2.8750 & 3.0068 & 2.9855 \end{bmatrix}, \tag{27b}$$

$$\Omega_{\text{opt}}^{\text{O}} = I_8 \times 39.35, \tag{27c}$$

where $I_7 = 800.0$ and $I_8 = 27.1$. Obviously, the estimated system matrix is optimized. Since I_8/I_6 is approximate to 2/3 which is consistent with the coefficient ratio calculated with Eqs. (10) or (11), we can say the total noise is dominant by the Gaussian noise. The main reason is that the photon flux of the system is low enough.

5. Discussions

5.1. Noise type

During deriving the analytical solution of the performance precision, we just consider Gaussian and Poisson noise respectively. Actually, the measurement also would be contaminated by other types of noise such as laser speckle noise, salt & pepper noise, uniform noise, or compound noise. It is complex and hard to derive the analytical solution of the estimation precision in the presence of those types of noise. However, we can add those noise into the intensities with Monte Carlo numerical simulation. It is found that the estimation precision are analogous to the case of the Gaussian or Poisson noise when using the optimal RPSs. That means the proposed RPSs are adaptive to the most types of noise or their combinations. This conclusion is verified in the experiments. For the strong light level, the experimental coefficient I_2 in Eq. (24b) is different from the theoretical one calculated from Eqs. (17) or (18). For the low light level, the experimental coefficient I_6 in Eq. (26b) is different from the theoretical one calculated from Eqs. (10) or (11). That
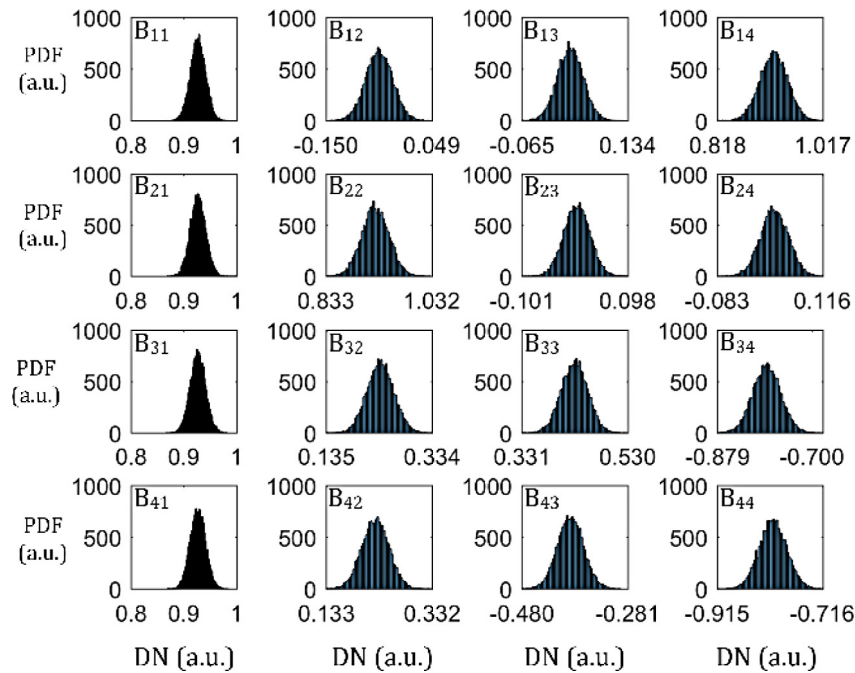
Fig. 6. The probability distributions functions (PDFs) of the elements of the estimated system matrix with normalized intensity.

means the noise in real system is not pure Poisson noise or Gaussian noise as assumed, it is the combination of different types of noise. However, it is easy to judge that Poisson noise is dominant in the strong light experiments and Gaussian noise is dominate in the low light experiments. No matter what type the noise is, the equalization and minimization of the noise variances can be achieved with the RPSs based on the *sphere* 3 *design* or *sphere* 2 *design* with the specific orientations.

5.2. Configurations of the PSG

Generally, the proposed optimal RPSs (sphere designs of order 2 or 3) can be generated with diverse PSG architectures. For example, an octahedron (sphere 3 design) can be generated with a linear polarizer at 0°, 90°, 45°, 135°, a right-circular polarizer and a left-circular polarizer [1,8,9]. However, since different polarization elements are needed, systematic errors would be introduced into the PSG with the exchange of polarization elements. Furthermore, the variation of optical flux introduced by different transmittance of elements would be misled as the effects of polarization modulation. Therefore, it is strongly suggested that the optimal sets of RPSs are generated with the same optical elements. The PSG setup proposed in Section 4 is easily configured with the off-the-shelf linear polarizer and QWPs. Actually, the mechanically rotating QWPs can be replaced by the ferroelectric liquid crystals to reduce systematic errors, since the retardation of the ferroelectric liquid crystal is constant, and the azimuth of its fast axis is driven electrically. The broadband optimally PSG based the ferroelectric liquid crystals would be the best choice for the calibration of the broadband PSA [2].

5.3. Systematic errors

During the derivation of the performance precision, we assume the PSA and PSG systems are perfect, and only consider the influence of noise. The numerical simulation using the parameters of perfect systems verified the feasibility of the proposed RPSs. However, both the PSA and PSG system matrices will deviate from the theoretical ones due to imperfect optical elements or alignment errors. Since the RPS calibration method has the potential of accounting for higher order effects of systematic errors in the PSA setup, we just need to

focus on the systematic errors in the PSG setup when the PSA setup is selected. In Section 43., we first use the standard polarimeter (Thorlabs, PAX1000VIS) to measure the real system matrix of the PSA and the real RPSs of the PSG. It is found that the real RPSs deviated from the ideal values a little bit. However, they are still considered as optimal RPSs. Fortunately, the system matrix estimated with the real RPSs approaches to that measured by the standard polarimeter (Thorlabs, PAX1000VIS). The noise variances of elements of the estimated system matrix are minimized and equalized. That means small systematic errors in the optimal PSG have no significant influence on the estimation. However, the acceptable maximum systematic error can be evaluated theoretically or numerically for the calibration of a practical PSA.

5.4. Number of RPSs

As we discussed in Section 2, the optimal sets of RPSs can be tetrahedron with $N_A = 4$ that belongs to sphere 2 designs, or octahedron with $N_A = 6$, cube with $N_A = 8$, icosahedron with $N_A = 12$ and dodecahedron with $N_A = 20$ that belong to the *sphere design* of order 3, or other regular polyhedrons with $N_A > 20$ that belong to the sphere t designs with $t \geq 3$. We can rotate the two QWPs in the proposed PSG setup to produce different sets of optimal RPSs respectively as shown in Table 2. Except for the tetrahedron with two specific orientations, the optimal sets of azimuths for octahedron or cube are diverse, that means other values that do not present in Table 2 also can be employed.

We should use at least four optimal RPSs to calibrate the full-Stokes PSA. The advantage of using fewer optimal RPSs is a reduction in measurement time for broadband systems or in systems with slow response times. Although fewer RPSs are easy to generate and time-saving, more RPSs could be employed to suppress the total noise variance and reduce the sensitivity of systematic errors [33,34] if the calibration time is a minor factor. According to the analytical solutions in Section 2, it is noted that the noise variance decreases with the increase of the number of the optimal RPSs when the numbers of the analysis states are fixed. This point is verified using Monte Carlo simulations with different numbers of RPSs in Section 3. Experimentally, the noise variance in the system matrix estimated with the octahedron of Eq. (22) is less than that estimated with the tetrahedron of Eq. (21). More importantly, for the same number of RPSs, the optimal sets of RPSs

can realize the minimization and equalization of the noise variance in the estimated system matrix compared to the nonoptimal sets of RPSs.

6. Conclusions

In summary, we have derived the analytical solution of the estimation variance of the system matrix, in the presence of Gaussian or Poisson noise, for the calibration of the PSA with the optimized RPSs. It is found that the optimal RPSs must form the regular polyhedrons of sphere *t* design on the Poincaré sphere of unit radius. Platonic solids such as tetrahedron, octahedron, cube, icosahedron and dodecahedron belong to the sphere designs of order 2 or 3. Wherein only tetrahedron belongs to spherical 2 design. If the RPSs form a general tetrahedron of spherical 2 design, the noise variances of the estimated system matrix will only be optimal for Gaussian noise. The noise variances will vary with the input signal if Poisson noise is dominant. However, if the RPSs form tetrahedrons with two special directions as shown in Table 2, the estimated system matrix will be optimal for both Gaussian and Poisson noise. That is the noise variances of the last three column for the estimated system matrix are equalized, the total noise variance is minimized, and the noise variances are independent of the input signal. Furthermore, if the RPSs form the polyhedrons of spherical 3 design, the estimated system matrix will always be optimized in the presence of both Gaussian and Poisson noise. The noise variances decrease with the increase of the numbers of the RPSs.

The analytical results are verified with the Mote Carlo simulations and practical experiments. In the experiments, we propose an easily realized architecture, a fixed linearly polarizer followed by two QWPs, for the generation of the regular polyhedrons based on *sphere design*. The sets of azimuths of the QWPs for tetrahedron, octahedron and cube are presented. The experimental results are consistent with the theoretical prediction even the practical noise is not the pure Gaussian or Poisson distribution. That is the proposed optimal RPSs are adaptive to the calibration of PSA in the presence of kinds of noise or their combinations.

The results shown in this paper are useful for the calibration of arbitrary Stokes polarimeter in linear optics with pseudo-inverse estimation and assess their fundamental limits in terms of estimation precision. Up to now, it can be concluded that, the PSA and PSG based on spherical designs of order 2 or 3 are the optimal configurations for the built of the Stokes polarimeter [12–19], and the built of Muller matrix polarimeter [20,21], and the calibration of the Stokes polarimeter presented in this paper. Although the presented method is developed for the calibration of Stokes polarimeters in linear optics, it can be extended for the calibration of nonlinear polarimetry in future.

References

[1] J.S. Tyo, D.L. Goldstein, D.B. Chenault, J.A. Shaw, Review of passive imaging polarimetry for remote sensing applications, Appl. Opt. 45 (2006) 5453–5469.

[2] Q. Liu, C. Bai, J. Liu, J. He, J. Li, Fourier transform imaging spectropolarimeter using ferroelectric liquid crystals and Wollaston interferometer, Opt. Express 25 (2017) 19904–19922.

[3] T. Mu, S. Pacheco, Z. Chen, C. Zhang, R. Liang, Snapshot linear-Stokes imaging spectropolarimeter using division-of-focal-plane polarimetry and integral field spectroscopy, Sci. Rep. 7 (2017) 42115.

[4] C.M. Persons, M.W. Jones, C.A. Farlow, L.D. Morell, M.G. Gulley, K.D. Spradley, A proposed standard method for polarimetric calibration and calibration verification, Proc. SPIE 6682 (2007) 66820K.

[5] B. Boulbry, J.C. Ramella-Roman, T.A. Germer, Improved method for calibrating a Stokes polarimeter, Appl. Opt. 46 (2007) 8533–8541.

[6] M. Gibney, Calibration of a visible polarimeter, Proc. SPIE 8364 (2012) 83640B.

[7] Joel G. Holder, Jacob A. Martin, Jeremey Pitz, Joseph L. Pezzaniti, Kevin C. Gross, Calibration methodology and performance characterization of a polarimetric hyperspectral imager, Proc. SPIE 9099 (2014) 90990J.

[8] Y. Zhang, H. Zhao, N. Li, Polarization calibration with large apertures in full field of view for a full Stokes imaging polarimeter based on liquid-crystal variable retarders, Appl. Opt. 52 (2013) 1284–1292.

[9] T. Mu, C. Zhang, R. Liang, Demonstration of a snapshot full-Stokes division-of-aperture imaging polarimeter using Wollaston prism array, J. Opt. 17 (2015) 125708.

[10] Olivier Morel, Ralph Seulin, David Fofi, Handy method to calibrate division-of-amplitude polarimeters for the first three Stokes parameters, Opt. Express 24 (2016) 13634–13646.

[11] G. Anna, F. Goudail, P. Chavel, D. Dolfi, On the influence of noise statistics on polarimetric contrast optimization, Appl. Opt. 51 (2012) 1178–1187.

[12] D.S. Sabatke, M.R. Descour, E.L. Dereniak, W.C. Sweatt, S.A. Kemme, G.S. Phipps, Optimization of retardance for a complete Stokes polarimeter, Opt. Lett. 25 (2000) 802–804.

[13] J.S. Tyo, Noise equalization in Stokes parameter images obtained by use of variable-retardance polarimeters, Opt. Lett. 25 (2000) 1198–1200.

[14] M.R. Foreman, A. Favaro, A. Aiello, Optimal frames for polarization state reconstruction, Phys. Rev. Lett. 115 (2015) 263901.

[15] H. Gu, X. Chen, H. Jiang, C. Zhang, S. Liu, Optimal broadband Mueller matrix ellipsometer using multi-waveplates with flexibly oriented axes, J. Opt. 18 (2016) 025702.

[16] F. Goudail, Equalized estimation of Stokes parameters in the presence of Poisson noise for any number of polarization analysis states, Opt. Lett. 41 (2016) 5772–5775.

[17] A. Peinado, A. Lizana, J. Vidal, C. Iemmi, J. Campos, Optimization and performance criteria of a Stokes polarimeter based on two variable retarders, Opt. Express 18 (2010) 9815–9830.

[18] T. Mu, Z. Chen, C. Zhang, R. Liang, Optimal configurations of full-Stokes polarimeter with immunity to both Poisson and Gaussian noise, J. Opt. 18 (2016) 055702.

[19] T. Mu, Z. Chen, C. Zhang, R. Liang, Optimal design and performance metric of broadband full-Stokes polarimeters with immunity to Poisson and Gaussian noise, Opt. Express 24 (2016) 29691–29704.

[20] G. Anna, F. Goudail, Optimal Mueller matrix estimation in the presence of Poisson shot noise, Opt. Express 20 (2012) 21331–21340.

[21] F. Goudail, Optimal Mueller matrix estimation in the presence of additive and Poisson noise for any number of illumination and analysis states, Opt. Lett. 42 (2017) 2153–2156.

[22] J.L. Pezzaniti, D. Chenault, M. Roche, J. Reinhardt, J.P. Pezzaniti, Four camera complete stokes imaging polarimeter, Proc. SPIE 6972 (2008) 69720J.

[23] G.R. Boyer, B.F. Lamouroux, B.S. Prade, Automatic measurement of the Stokes vector of light, Appl. Opt. 18 (1979) 1217–1219.

[24] S.X. Wang, A.M. Weiner, Fast wavelength-parallel polarimeter for broadband optical networks, Opt. Lett. 29 (2004) 923–925.

[25] X. Zhao, A. Bermak, F. Boussaid, V.G. Chigrinov, Liquid-crystal micropolarimeter array for full Stokes polarization imaging in visible spectrum, Opt. Express 18 (2010) 17776–17787.

[26] G. Myhre, W.-L. Hsu, A. Peinado, C. LaCasse, N. Brock, R.A. Chipman, S. Pau, Liquid crystal polymer full-stokes division of focal plane polarimeter, Opt. Express 20 (2012) 27393–27409.

[27] P. Llull, G. Myhre, S. Pau, Lens array Stokes imaging polarimeter, Meas. Sci. Technol. 22 (2011) 065901.

[28] A.N. Langville, W.J. Stewart, The Kronecker product and stochastic automata networks, J. Comput. Appl. Math. 167 (2004) 429–447.

[29] A. Ambirajan, D.C. Look, Optimum angles for a polarimeter: part I, Opt. Eng. 34 (1995) 1651–1655.

[30] H. Gu, S. Liu, X. Chen, C. Zhang, Calibration of misalignment errors in composite waveplates using Mueller matrix ellipsometry, Appl. Opt. 54 (2015) 684–693.

[31] H. Gu, X. Chen, H. Jiang, C. Zhang, W. Li, S. Liu, Accurate alignment of optical axes of a biplate using a spectroscopic Mueller matrix ellipsometer, Appl. Opt. 55 (2016) 3935–3941.

[32] W. Li, C. Zhang, H. Jiang, X. Chen, S. Liu, Depolarization artifacts in dual rotating compensator Mueller matrix ellipsometry, J. Opt. 18 (2016) 055701.

[33] J.S. Tyo, Design of optimal polarimeters: maximization of signal-to-noise ratio and minimization of systematic error, Appl. Opt. 41 (2002) 619–630.

[34] J.S. Tyo, H. Wei, Optimizing imaging polarimeters, constructed with imperfect optics, Appl. Opt. 45 (2006) 5497–5503.